JOURNAL OF GEOPHYSICAL RESEARCH, VOL. 88, NO. A9, PAGES 7059–7064, SEPTEMBER 1, 1983

Standing Wave Patterns in VLF Hiss

R. BRITTAIN, P. M. KINTNER, AND M. C. KELLEY

School of Electrical Engineering, Cornell University

J. C. SIREN[1]

Institute for Physical Science and Technology, University of Maryland

D. L. CARPENTER

Space, Telecommunications, and Radioscience Laboratory, Stanford University

Observations have been made of systematic patterns in VLF hiss, which can be interpreted as a standing wave pattern formed by reflection in the lower ionosphere. Multicomponent VLF electric and magnetic field experiments were flown on three sounding rockets (Nike-Tomahawk 18.203-205) from Siple Station. Antarctica during December 1980 to January 1981. One feature of the natural emissions was observed in a very similar form during each flight. A band of hiss, typically from 1.5 to 3 kHz, was seen on the upleg to form a series of closely spaced stripes with whistler-like dispersion. These first appeared at an altitude of 90–95 km and extended for as much as 40 km in altitude. On the downleg the stripes were observed at the same altitude with the pattern reversed in time. No such patterns were observed by the VLF receivers operating at the same time on the ground at Siple or at its conjugate point. It is suggested that the patterns are interference effects due to downcoming waves reflecting from a layer in the E region and forming a standing wave pattern. The observed stripes are then due to the rocket traversing the standing wave pattern in opposite directions on upleg and downleg. If this interpretation is correct, the fringe spacing should be related to the wavelength and permits a calculation of the refractive index. In one example we calculate $n = 43.7$ in good agreement with two independent determinations of the refractive index.

INTRODUCTION

The propagation of whistler mode waves in magnetized plasmas with slowly varying parameters has been studied in the magnetosphere for decades and has largely been verified by experiment. At the interface of neutral atmosphere and ionosphere, however, plasma parameters do not vary slowly compared to the wavelength of whistler mode waves and a combihation of reflection, absorption, and transmission should occur across the interface. Evidence that whistler mode waves incident from above the interface do reflect has been provided by multiple hop whistlers, multihop fixed frequency transmitter signals, and natural periodic emissions [*Helliwell*, 1965], as well as by satellite whistler observations [*Gurnett et al.*, 1971; *Thomson and Dowden*, 1977]. Various properties of the observed waves suggest that reflection occurs at around 100 km altitude; an example is the observation on a rocket of multiple 'subprotonospheric' whistler components in the 100–200 km altitude range [*Carpenter et al.*, 1964]. Full-wave calculations of internal reflection coefficients for downcoming whistler mode waves also support reflection at the interface, particularly in the presence of a sporadic E layer [*Pitteway and Jesperson*, 1966].

In this paper we report the observation of some unusual VLF electric and magnetic fluctuations measured from three sounding rockets in the altitude range 90–140 km. The characteristic signature is broadband hiss in the range 1.3–3.5 kHz exhibiting amplitude 'stripes' on a conventional sonogram. The dispersive frequency-time structure of these stripes was reversed in time as the rocket traversed the same altitude region in the reverse direction (on the downleg). This may be understood if we interpret the stripes as a spatial interference pattern through which the rocket flies. Assuming a single wave vector direction for the incident (downcoming) VLF waves, reflection from a sharp gradient of refractive index will produce a standing wave pattern by interference of incident and reflected waves above the reflection layer.

ELF/VLF hiss is believed to originate just inside the plasmapause at high altitudes [*Thorne et al.*, 1973, 1977]. Low-altitude measurements of VLF hiss by polar orbiting satellites show that the maximum probability of occurrence is located near local noon and near $L = 4$, conditions pertaining to all three of the flights [*Taylor and Gurnett*, 1968]. From such studies we may conclude that the observed hiss probably originated at high altitude, near the magnetic equator, and propagated downward to the rocket in the lower ionosphere, where it is reflected. The reflection process may then contribute substantially to establishing VLF hiss amplitudes. Similar stripes in ELF hiss ($f < 1$ kHz) may have been observed on a sounding rocket flown at much higher magnetic latitude, into the dayside auroral oval (M. Temerin, private communication, 1982).

These observations were made from three Nike-Tomahawk sounding rockets (flights 18.203–18.205) launched from Siple station, Antarctica ($L = 4.3$) during a variety of geophysical conditions. An overview article by *Matthews* [1981] describes the campaign in general. The payloads reached an altitude of about 200 km during a flight of about 360 s. VLF instrumentation was identical on each of the payloads, consisting of three perpendicular loop antennas to

[1] Now at Lincoln Laboratory, Massachusetts Institute of Technology.

Paper number 3A0807.
0148-0227/83/003A-0807$05.00

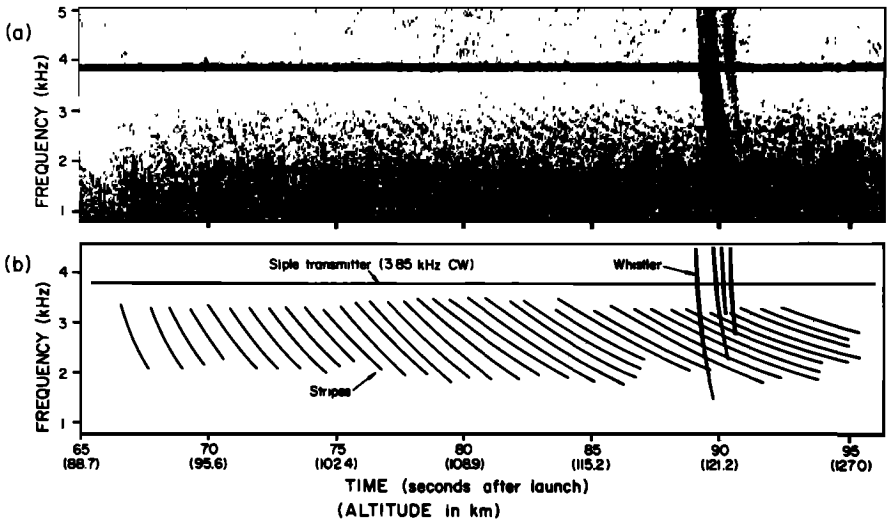

Fig. 1. Flight 18.205 upleg stripes. (*a*) Sonogram of the magnetic x channel. (*b*) Line drawing showing the position of the stripes in Figure 1*a* and identifying the Siple transmitter and a coincidental whistler at 90 s.

measure ac magnetic fields, and two crossed 3-m double probes terminated with spheres and separated along the rocket axis direction, to measure dc and ac electric fields. The electric field channels had flat response over the range 30 Hz to 8 kHz, while the magnetic field channels were peaked at 4 kHz and emphasized the band 1–7 kHz. A digital automatic gain control (AGC) with dynamic range greater than 70 dB was used on all channels. The broadband outputs were transmitted to ground, digitized, and analyzed by using standard digital signal processing techniques.

Experimental Observation of Stripes

Figure 1 shows an example of 'stripes' in the upper panel, taken from a portion of the upleg of flight 18.205 as it entered the ionosphere. The lower panel is a schematic outline identifying the various features. Since the AGC level was set by the strongest signal in the receiver passband (in this case the Siple transmitter), none of the examples have optimum gain setting and most are close to the receiver sensitivity threshold. During this flight (18.205), geomagnetic conditions were favorable for amplifying the Siple transmissions and producing echoes, but very little natural VLF was observed, with the exception of some low-intensity VLF hiss and occasional discrete emissions in the range 1–3 kHz. The stripes begin at 90 km and continue to above 140 km in altitude, and show a whistlerlike dispersion with a spacing in altitude of (very approximately) 1 km. The CW tone at 3.85 kHz is due to the Siple transmitter. It is discussed in a companion paper [*Kintner et al.*, this issue]. The pattern of stripes was common to the upleg of each flight, whether or not the Siple transmitter was operating.

An example of downleg stripes is shown in Figure 2, taken from flight 18.204 which was launched in an intense chorus event. The chorus and hiss were predominantly in the ranges 0.8–1.5 kHz and 3–5 kHz. The stripes are visible in the lower panel, between 1.4 and 3 kHz, and slope upward to the right, becoming more vertical with time. The upper panel of Figure

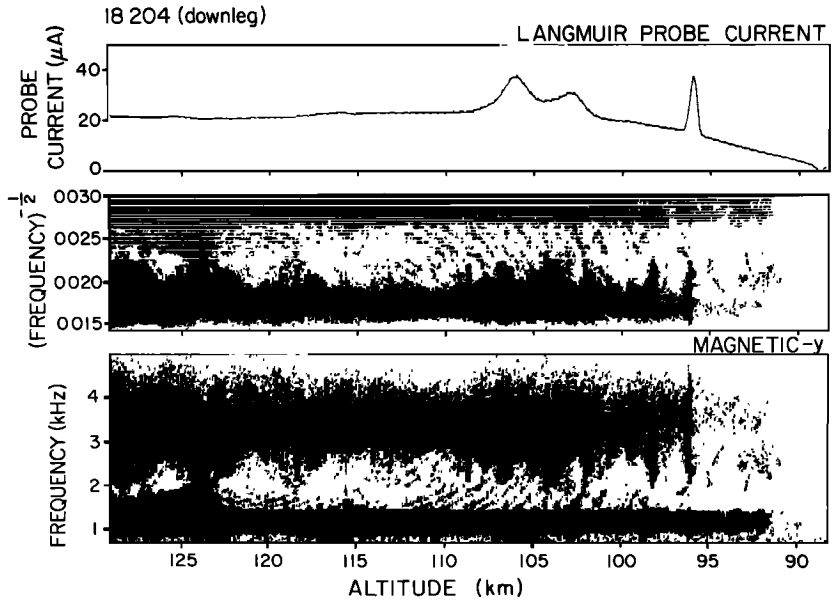

Fig. 2. 18.204 downleg data. (top) Langmuir probe data with 0.288 s averaging time. (middle) $1/(f)^{1/2}$ spectrogram of B_y. (bottom) Sonogram of B_y-linear height scale.

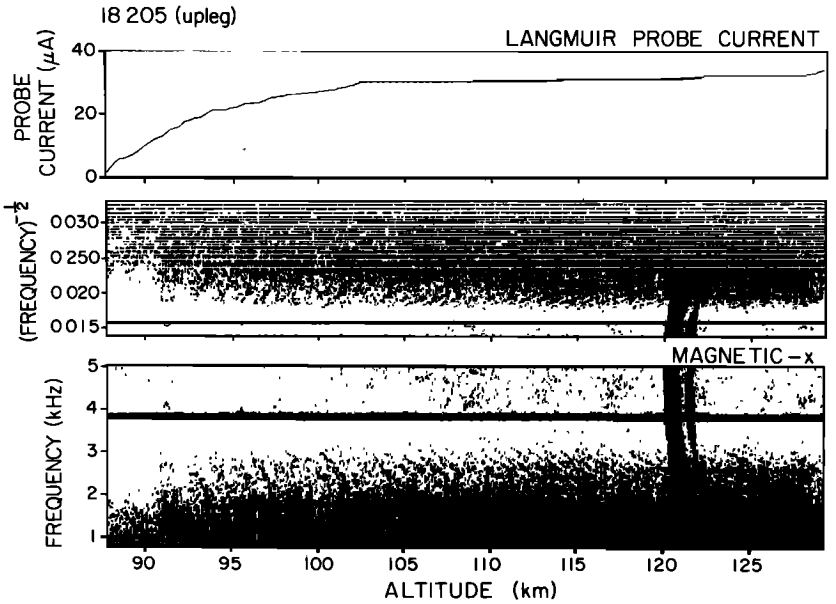

Fig. 3. 18.205 upleg data. (top) Langmuir probe data with 0.288 s averaging time. (middle) $1/(f)^{1/2}$ spectrogram of B_x. (bottom) Sonogram of B_x-linear height scale.

2 shows the current drawn by a Langmuir probe operated in the electron saturation regime (probe current is proportional to electron density). Within the E region three electron density enhancements occurred; these appear also on the upleg measurements and are believed to be caused by shears in the neutral wind [*Chimonas and Axford*, 1968]. The third enhancement at 96 km corresponds to a factor of 3 increase in electron density over an altitude range less than the stripe spacing, and occurs approximately at the altitude at which the stripes become vertical and cease. The middle panel shows the same data as the lower panel except that the ordinate is now proportional to $1/(f)^{1/2}$instead of f (low frequencies toward the top of the panel and high frequencies toward the bottom; note that the white bands are an artifact of the frequency inverting program). This choice of frequency scale 'linearizes' the stripes if the wavelength varies as $1/(f)^{1/2}$ (whistler mode dispersion). The stripes now appear as nearly straight lines directed towards a common origin at infinite frequency. Over this short section of flight, time, and altitude are roughly proportional and the abscissa has been adjusted to be linear with altitude. In Figure 3 the data of Figure 1 have been replotted in the format of Figure 2. The electron density rises monotonically through the E region with no enhancements. In the middle panel the sign of the slopes is opposite to that of Figure 2 and the apparent origin appears to be about 90 km where the electron density is changing rapidly.

The above two examples were chosen for detailed study. Table 1 summarizes the observed properties of all events on flights 18.203, 18.204, and 18.205. Since the stripes are close to receiver sensitivity, estimates of duration and amplitude are somewhat approximate. For example, the lack of electric field observations in three of the five examples is most likely a result of the sensitivity threshold. Perhaps the most surprising aspect of Table 1 is the observation of stripes on every rocket flight. This phenomenon appears to be a common feature of the lower ionosphere during periods of VLF activity. Although the nature of the activity varied from

TABLE 1. Summary of Observations of 'Stripes'

Flight	18.203	18.203	18.204	18.204	18.205	18.205
Launch time, UT	1719:44.5		1732:36.2		1822:18.2	
Date	Dec. 8, 1980		Dec. 20, 1980		Jan. 10, 1981	
Leg observed	up	down	up	down	up	down
Altitude of lowest fringe, km	88 ± 1	88 ± 1	101 ± 1	96 ± 1	90 ± 1	. . .
Time duration, s	18	33	15	37	50	. . .
Height range, km	25	45+	18	43+	55+	. . .
Total number of fringes observed	15	30+	10	40+	40+	. . .
Frequency range, kHz	1.2–2.8		1.4–3.0		1.5–3.6	
Identified in magnetic	yes	yes	yes	yes	yes	no
Identified in electric	no	yes	no	yes	no	no
Spacing in time at constant frequency, s (very approximately)	1	1	1	1	1	. . .
Dynamic range (maxima-minima), dB	. . .	. . .	. . .	<10	<10	. . .
Amplitude of maxima mγ $Hz^{1/2}$	. . .	. . .	. . .	0.085	0.05	. . .

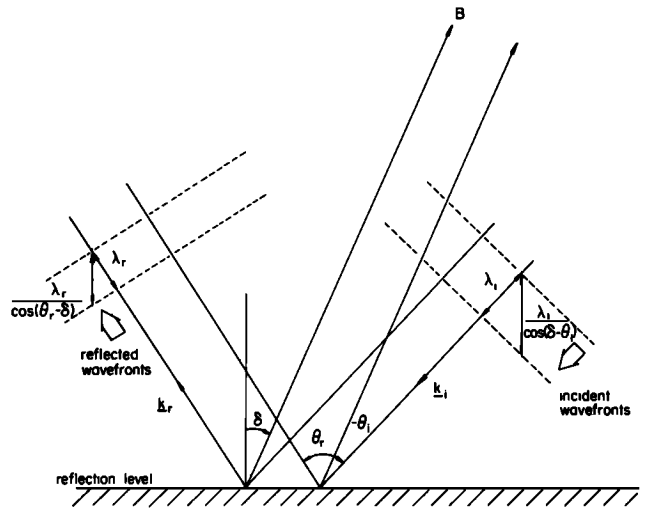

Fig. 4. Geometry for incident wave at angle θ_i to the geomagnetic field, and reflected wave at angle θ_r.

flight to flight, each flight took place during a period when the Siple signal was being amplified and observed either as a one-hop signal at the conjugate station Roberval or as a two-hop echo at Siple. In no instance were similar stripes being observed in the ground VLF records at Siple or its conjugate point.

INTERPRETATION

The VLF signals described in this paper are propagating at frequencies much greater than the ion cyclotron frequency (20 Hz). In this regime the index of refraction of a whistler mode wave can be accurately approximated as

$$n^2 = \frac{f_{pe}^2}{f f_{ge} \cos \theta} \tag{1}$$

where f_{pe} is plasma frequency and f_{ge} is electron gyrofrequency and θ is the angle between the wave vector and the magnetic field (see Figure 8). This is a quasi-longitudinal approximation but in the regime considered here is valid for angles up to 80° or more.

The condition for destructive interference producing a null in the standing wave pattern is that the phase path difference between direct and reflected signal should be an odd integer multiple of π. If the vertical gradient of refractive index is great enough we may assume a sharp reflecting layer and use graphical methods for obtaining the reflected wave-vector and ray directions. Figure 4 shows the geometry for geomagnetic field B_0 at angle δ to vertical, incident wave at angle θ_i, and reflected wave at angle θ_r to B_0. The phase difference between direct and reflected waves at height h above the reflecting layer is then given by

$$\Delta\phi = k_i h \cos(\delta - \theta_i) + k_r h \cos(\theta_r - \delta) \tag{2}$$

where $k(\omega, \theta_{i,r})$, the wave number, is different for incident and reflected rays because the wave vector angle will in general be different. With the refractive index approximation used here, θ_r is a function only of θ_i and δ. At sufficiently high frequencies or large wave normal angles, the reflected ray direction will also be frequency dependent, and this would distort the stripe pattern from the hyperbolic shape observed. The condition for an interference null may be written as

$$\Delta\phi = (2n + 1)\pi \qquad n = 0, 1, 2, 3, \cdots$$

Substituting the above expression for refractive index and rearranging gives the following relationship beteen frequency and altitude above the reflecting layer, for a null of order n:

$$h(f)^{1/2} = \frac{(2n + 1)c(f_{ge})^{1/2}}{2f_{pe}} \cdot \left[\frac{(\cos\theta_i \cos\theta_r)^{1/2}}{\cos(\delta - \theta_i)(\cos\theta_r)^{1/2} + \cos(\theta_r - \delta)(\cos\theta_i)^{1/2}}\right] \tag{3}$$

We can now comment on the specific characteristics of the stripes in Figures 1, 2, and 3. If the incident waves have a constant wave vector direction and the refractive index is constant (or approximately so), the right side of equation (3) becomes a constant for a given null (fixed n) and hence $1/(f)^{1/2}$ becomes a linear function of altitude, or on a conventional sonogram, a set of hyperbolic curves is produced. Close to the reflection level, the stripes are nearly vertical, becoming more horizontal with increasing height. As can be seen in Figures 2 and 3, the electron density is approximately constant beyond a few fringes above the reflection level, and the middle panels show straight lines as expected. Figure 5 shows the 18.205 upleg stripes plotted as $1/(f)^{1/2}$ versus altitude with straight lines fitted through the nulls and extrapolated back to infinite frequency ($1/(f)^{1/2} = 0$), which should give the reflection height ($h = 0$) for each fringe. The fitted lines intersect at 90 km, the altitude of the reflection level. The reciprocal slopes of these lines were plotted against $(2n + 1)$, where n is the null index, in Figure 6. The

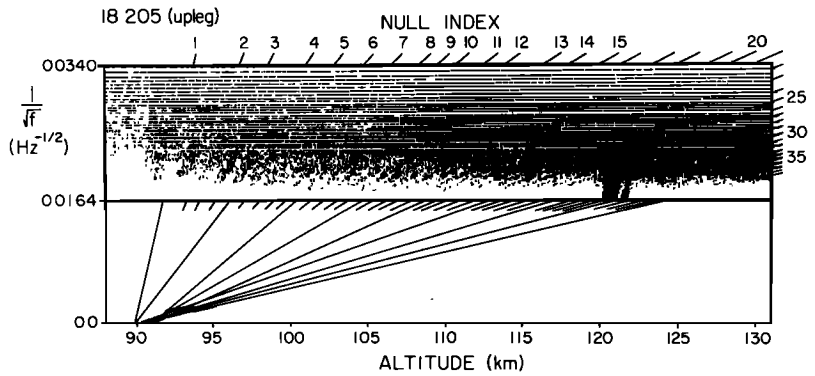

Fig. 5. $1/(f)^{1/2}$ spectrogram of 18.205 upleg showing graphical technique for determining reflection height.

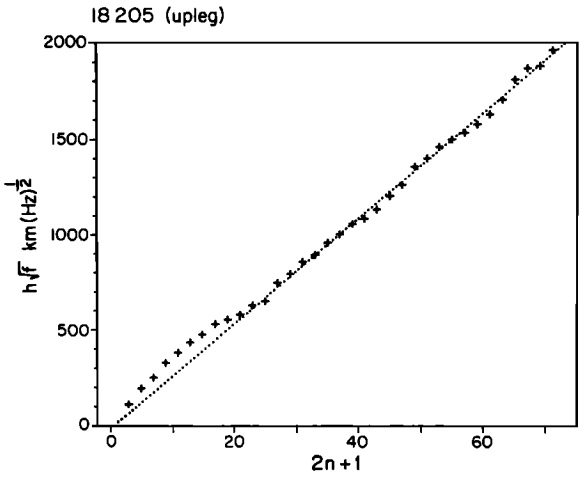

Fig. 6. Plot of $h(f)^{1/2}$ versus $(2n + 1)$ for the stripes of 18.205 upleg. Fitted line uses only fringes 11–35 (above ~105 km where density is roughly constant).

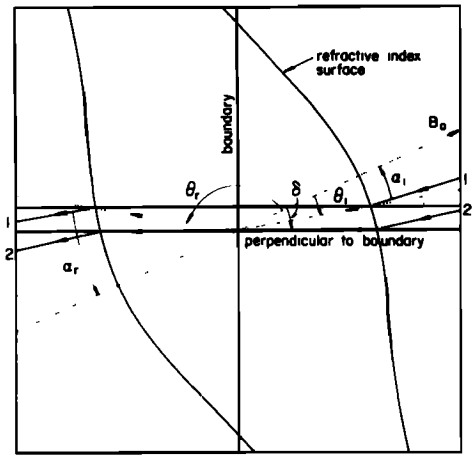

Fig. 8. Refractive index surface for whistler mode waves above the reflection level. Axis of symmetry is magnetic field direction. Representative waves plotted are for (curve 1) $\theta_i = 14°$ and (curve 2) $\theta_i = 24°$ (vertical wave normal).

best fit straight line through these points gives a value for f_{pe} from equation (3), averaged over the height interval 105–130 km (only those fringes for which the Langmuir probe indicates roughly constant electron density were used). The angle dependent factor in (3) will be seen to be relatively unimportant for estimating f_{pe}.

For the 18.204 downleg, the height per fringe was carefully measured and a relative electron density profile deduced (relative, since the angles are not known), shown in Figure 7. This reproduces the general shape of the Langmuir probe data over the same height interval.

The problem of calculating the reflected wave ray path and wave normal angle is solved graphically with the aid of a refractive index surface and Snell's law [see *Helliwell*, 1965]. For simplicity, we assume the axis of symmetry of the medium (direction of B_0) to lie in the plane of propagation. Figure 8 shows the refractive index surface for the ionosphere above the reflection level (assumed horizontal), for a magnetic dip angle of 66°. With the refractive index approximation used here the shape of the surface is determined only by the cos θ factor, and so the assumed values of f_{pe} and f_{ge} do not affect the construction of the reflected angles. A line is drawn from the origin O in the direction of the incident wave θ_i, and the perpendicular to the surface at the intersection with this line gives the incident ray direction (group ray velocity direction). By Snell's law the refractive index vector $\mathbf{n}(= n\mathbf{k}/k)$ of the reflected wave must have the same projection in the boundary as that of the incident wave, and hence a line perpendicular to the boundary will intersect the surface at all possible refractive index vector terminations. The reflected wave direction can thus be drawn in at angle θ_r, and again the perpendicular to the surface gives the ray direction. Note that in general the angle of incidence is not equal to the angle of reflection. The angle factor of equation (3) may now be evaluated as a function of incident wave normal angle. Figure 8 shows the construction for incident wave normals vertical ($\theta_i = 24°$) and near vertical, and Figure 9 shows the corresponding ray paths. Note that a vertical incident wave normal is the only geometry in which the wave normal and ray directions are unchanged under the reflection. The reflected ray is collinear with the incident ray and the reflected wave normal is collinear with the incident wave normal. Since the signals were very weak, it was not possible to measure the wave normal angles even with full six-component instrumentation; however, on 18.205 the stripes were not observed on the rocket B_z component (the rocket axis was parallel to B_0 on this flight). This suggests a nearly vertical wave normal, since this would give the smallest B_z component for both direct and reflected waves (possibly present but below the receiver sensitivity). The angle-dependent factor in equation (3) does not vary by more than 7% over the range $\theta_i = -10°$ to $+50°$, so the exact angle assumed is not critical. Taking a vertical wave normal ($\theta_i = 24°$ for the Siple dip angle of 66°) allows an estimate of mean electron density from Figure 6 of 1.24×10^5 cm^{-3}. Since we are assuming a vertical wave normal for the hiss, we may compare the calculated refractive index with that measured for the Siple transmitter signal (which must be propagating from below at an angle very close to vertical, by Snell's law). The above electron density gives a refractive index of 42.7 for 3.85 kHz (the transmitter frequency), which compares well with values of 40 obtained by a Doppler/interferometer

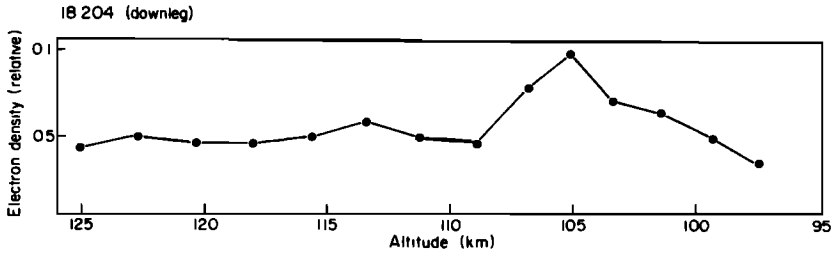

Fig. 7. 18.204 downleg. Electron density profile derived from fringe spacing.

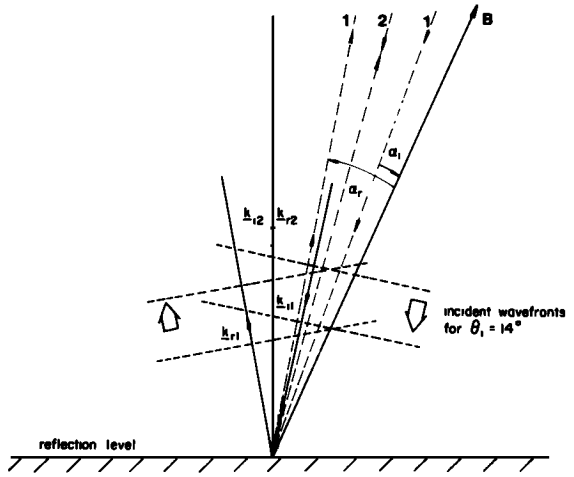

Fig. 9. Ray and wave normal directions for wave normal angles close to vertical; (curve 1) $\theta_i = 14°$ and (curve 2) $\theta_i = 24°$ (vertical wave normal). Dashed lines 1 and 2 are the associated ray directions.

technique and 55 obtained by a direct measurement of the ratio *B/E* for the transmitter. These latter values are discussed further in a separate paper [*Kintner et al.*, this issue]. Applying the same argument to the downleg of 18.204 gives a mean density of 1.8×10^5 cm^{-3} for heights above 107 km.

An estimate of the allowable width of the wave normal angle distribution function was made by plotting equation (3) for various distributions of incident angles. If the incident wave normal angle is outside the range −20° to +50° the angle factor (square brackets) is a rapidly varying function and this causes the stripes to merge together for an angular spread of >6° (standard deviation) and order $n > 4$–5. For small wave normal angles, a wider spread in wave normal angles is possible; for 24°, the stripes are distinct to order >20 and spread ≅ 15°. This tends to confirm that the observed stripes are due to hiss with a small range of wave normal angles about a value close to vertical.

SUMMARY

An interference pattern caused by reflection of broadband VLF hiss from a fairly sharp layer at about 90 km altitude has been observed on a rocket on both upleg and downleg of two flights and on the upleg of a third flight. The observed fringe spacing, related to the local wavelength of the VLF waves, gave plausible estimates of electron density, in one case well supported by two completely independent measurements at the same point in the flight. We infer from these results the presence of a refractive index gradient sufficiently sharp that the reflection may be assumed specular, and a constant (or almost so) wave vector direction for the incident waves.

A critical factor in the observation of this interference pattern is the distribution of wave normal angles present in the hiss. Most experiments to measure wave normals for natural VLF have relied on assumptions of a single plane wave [e.g., *Mosier and Gurnett*, 1971] and hence have not been able to measure distributions. *Altman et al.* [1975] inferred the occurrence of a restricted range of wave vectors in ELF hiss from theoretical (full wave) calculations. *Lefeuvre et al.* [1981, 1982] have successfully measured the wave distribution functions for broadband hiss observed on the GEOS 1 satellite and found typically two separate and well defined angles for each example of natural emissions. From the visibility of interference fringes in these experiments to quite large orders, we conclude that the distribution of wave normal directions is very narrow.

Acknowledgments. We would like to thank the project scientist David Matthews for his support throughout all aspects of the campaign, also John Katsufrakis for help in preparing analogue spectrograms used in compiling Table 1, and Michael Rycroft and Timothy Bell for valuable discussion. This research was supported by the Division of Polar Programs of the NSF under grant DPP-80-23968 at Cornell, and under grants DPP-8022282 and DPP-8022540 at Stanford.

The Editor thanks S. Church and R. L. Dowden for their assistance in evaluating this paper.

REFERENCES

Altman, C., H. Cory, S. Zorea, and E. Fijalkow, A full-wave study of downward propagating ELF waves in the ionosphere: ion cutoff whistlers and the low frequency cutoff of ELF noise, *Planet. Space Sci., 23,* 1155, 1975.

Carpenter, D. L., N. Dunckel, and J. F. Walkup, A new very low frequency phenomenon: Whistlers trapped below the protonosphere, *J. Geophys. Res., 69,* 5009, 1964.

Chimonas, G., and W. I. Axford, Vertical movement of temperate-zone sporadic *E* layers, *J. Geophys. Res., 73,* 111, 1968.

Gurnett, D. A., S. R. Mosier, and R. R. Anderson, Color spectrograms of very low frequency Poynting flux data, *J. Geophys. Res., 76,* 3022, 1971.

Helliwell, R. A., *Whistlers and Related Ionospheric Phenomena,* Stanford University Press, Stanford, Calif., 1965.

Kinter, P. M., R. Brittain, M. C. Kelley, D. L. Carpenter, and M. J. Rycroft, In situ measurements of transionospheric VLF wave injection, *J. Geophys. Res.,* this issue.

Lefeuvre, F., M. Parrot, and C. Delannoy, Wave distribution functions estimation of VLF electromagnetic waves observed onboard GEOS 1, *J. Geophys. Res., 86,* 2359, 1981.

Lefeuvre, F., T. Neubert, and M. Parrot, Wave normal directions and wave distribution functions for ground based transmitter signals observed on GEOS 1, *J. Geophys. Res., 87,* 6203, 1982.

Matthews, D. L., Siple station magnetospheric physics campaign, *Antarct. J. U.S., 16*(5), 202–203, 1981.

Mosier, S. R., and D. A. Gurnett, Theory of the INJUN 5 Poynting flux measurements, *J. Geophys. Res., 76,* 972, 1971.

Pitteway, M. L. V., and J. L. Jesperson, A numerical study of the excitation, internal reflection and limiting polarization of whistler waves in the lower inosphere, *J. Atmos. Terr. Phys., 28,* 17–43, 1966.

Taylor, W. W. L., and D. A. Gurnett, Morphology of VLF emissions observed with the INJUN 3 satellite, *J. Geophys. Res., 73,* 5615, 1968.

Thomson, R. J., and R. L. Dowden, Simultaneous ground and satellite reception of whistlers, 1, Ducted whistlers, *J. Atmos. Terr. Phys., 39,* 869, 1977.

Thorne, R. M., E. J. Smith, R. K. Burton, and R. E. Holzer, Plasmaspheric hiss, *J. Geophys. Res., 78,* 1581, 1973.

Thorne, R. M., S. R. Church, W. J. Malloy, and B. T. Tsurutani, The local time variation of ELF emissions during periods of substorm activity, *J. Geophys. Res., 82,* 1585, 1977.

R. Brittain, M. C. Kelley, and P. M. Kintner, School of Electrical Engineering, Cornell University, Ithaca, NY 14853.

D. L. Carpenter, Space, Telecommunications, and Radioscience Lab, Stanford University, Stanford, CA 94305.

J. C. Siren, Lincoln Laboratory, Massachusetts Institute of Technology, Lexington, MA 02173.

(Received February 2, 1983;
revised May 16, 1983;
accepted May 19, 1983)